

Nonlinear diffusion filtering of data on the Earth's surface

Róbert Čunderlík, Karol Mikula & Martin Tunega

Journal of Geodesy

Continuation of Bulletin Géodésique and manuscripta geodaetica

ISSN 0949-7714

Volume 87

Number 2

J Geod (2013) 87:143-160

DOI 10.1007/s00190-012-0587-y



Your article is protected by copyright and all rights are held exclusively by Springer-Verlag. This e-offprint is for personal use only and shall not be self-archived in electronic repositories. If you wish to self-archive your work, please use the accepted author's version for posting to your own website or your institution's repository. You may further deposit the accepted author's version on a funder's repository at a funder's request, provided it is not made publicly available until 12 months after publication.

Nonlinear diffusion filtering of data on the Earth's surface

Róbert Čunderlík · Karol Mikula · Martin Tunega

Received: 12 January 2012 / Accepted: 6 August 2012 / Published online: 7 September 2012
© Springer-Verlag 2012

Abstract The paper deals with data filtering on closed surfaces using linear and nonlinear diffusion equations. We define a surface finite-volume method to approximate numerically parabolic partial differential equations on closed surfaces, namely on a sphere, ellipsoid or the Earth's surface. The closed surface as a computational domain is approximated by a polyhedral surface created by planar triangles and we construct a dual co-volume grid. On the co-volumes we define a weak formulation of the problem by applying Green's theorem to the Laplace–Beltrami operator. Then the finite-volume method is applied to discretize the weak formulation. Weak forms of elliptic operators are expressed through surface gradients. In our numerical scheme we use a piece-wise linear approximation of a solution in space and the backward Euler time discretization. Furthermore, we extend a linear diffusion on surface to the regularized surface Perona–Malik model. It represents a nonlinear diffusion equation, which at the same time reduces noise and preserves main edges and other details important for a correct interpretation of the real data. We present four numerical experiments. The first one has an illustrative character showing how an additive noise is filtered out from an artificial function defined on a sphere. Other three examples deal with the real geodetic data on the Earth's surface, namely (i) we reduce a stripping noise from the GOCE satellite only geopo-

tential model up to degree 240, (ii) we filter noise from the real GOCE measurements (the component T_{zz}), and (iii) we reduce a stripping noise from the satellite only mean dynamic topography at oceans. In all experiments we focus on a comparison of the results obtained by both the linear and nonlinear models presenting advantages of the nonlinear diffusion.

Keywords Data filtering on a closed surface · Linear and nonlinear diffusion equations · Surface finite volume method · Surface gradients · The regularized surface Perona–Malik model

1 Introduction

Data filtering has become an essential part of processing various kinds of measurements that contain noise and other inaccuracies. In many applications, a quality of filtering has obvious impact on correct interpretations of obtained results. During the last decades there have been developed many efficient filters that can reduce noise from observed data. The filters usually used for processing measurements in geodesy are mostly based on linear filtering, e.g. Gaussian, Wiener or Kalman filters, considered either in frequency or space domain. However, the linear filtering is based on uniform smoothing, which at the same time smoothes main structures in the signal losing important information about these characteristics.

On the contrary, the nonlinear diffusion filtering allows non-uniform smoothing that can be locally adapted to data features, e.g. according to local gradients or curvature of the noisy data. Such adaptive smoothing effect has an advantage that main structures or edges can be preserved while the noise can be effectively reduced. A need of optimal nonlinear filters underlines a fact that most physical systems in nature are

R. Čunderlík (✉) · K. Mikula · M. Tunega
Department of Mathematics and Descriptive Geometry,
Faculty of Civil Engineering, Slovak University of Technology,
Radlinského 11, 813 68 Bratislava, Slovakia
e-mail: cunderli@svf.stuba.sk

K. Mikula
e-mail: mikula@math.sk

M. Tunega
e-mail: martin.tunega@gmail.com

inherently nonlinear. Therefore recently developed nonlinear filters like the particle filters, extended Kalman filters, batch filters, exact recursive filters and others have become popular in many practical applications.

In this paper we focus on filtering methods mostly used in image processing that are based on the partial differential equations (PDEs) approach (cf. Alvarez et al. 1993; Mikula and Ramarosy 2001; or Mikula 2002). The first step to use PDEs for image processing was done at the beginning of the 80's (Witkin 1983; Koenderink 1984). By the simple observation that the Gauss function is a fundamental solution of the linear heat (diffusion) equation, it has been possible to replace the classical operation—convolution of an image with the Gauss function (Gaussian smoothing)—by solving the linear diffusion equation for a corresponding time with an initial condition given by the processed image. It has been well known that Gaussian smoothing (linear diffusion) blurs edges in the image and moves their positions. To overcome this drawback, the nonlinear diffusion models started to be developed.

Since the end of the 80's, the nonlinear diffusion equations have been used for processing of 2D or 3D images. After the pioneering work of Perona and Malik (1987), who modified the linear heat equation to a nonlinear diffusion preserving edge positions, there has been a great deal of interests in applications and analysis of such equations. At present, there are known at least two basic nonlinear diffusion approaches; (i) the regularized Perona–Malik model, where the diffusion coefficient depends on an edge detector (Catté et al. 1992), and (ii) the geodesic mean curvature flow model based on a geometrical diffusion of level-sets of the image intensity (Caselles et al. 1995, 1997; Kichenassamy et al. 1995, 1996, or Chen et al. 2000).

The aim of this paper is to present mathematical models and numerical methods for solving the linear and nonlinear diffusion equations considered on a closed surface like a sphere, ellipsoid or the Earth's surface. We introduce finite volume schemes to obtain numerical solutions of these parabolic PDEs on closed surfaces. In case of the nonlinear surface diffusion we use the regularized surface Perona–Malik model. Presented filtering methods represent original approaches from the geodetic as well as mathematical point of view. Another approach based on surface finite elements for the parabolic PDEs including a detailed mathematical background is described in Dziuk and Elliott (2007).

2 The linear diffusion on a closed surface

Conservation of a scalar quantity u on a closed surface Γ with a diffusive flux $-\lambda \nabla_S u$, where λ is the diffusivity coefficient, leads to the diffusion equation

$$\frac{\partial u}{\partial t} - \nabla_S \cdot (\lambda \nabla_S u) = 0 \tag{1}$$

on Γ (Dziuk and Elliott 2007), where ∇_S represents a tangential or surface gradient. For simplicity we consider $\lambda \equiv 1$. Then Eq. (1) can be written in the form

$$\frac{\partial u}{\partial t} - \Delta_S u = 0, \tag{2}$$

where Δ_S is the Laplace–Beltrami operator, which represents the generalized Laplace operator defined on a surface. The parabolic PDE (2) represents the surface linear diffusion and corresponds to the heat equation on a closed surface. In case that Γ is a closed surface in 3D, Eq. (2) does not need a boundary condition.

3 The surface finite volume method for the linear diffusion

In order to approximate numerically the linear diffusion equation (2) on the closed surface Γ , we define a surface finite volume method (SFVM). At first, the computational domain Γ is approximated by a polyhedral surface using an appropriate triangulation. An example of the triangulation of a sphere is shown in Fig. 1, where the representative nodes X_i ($i = 1, \dots, N$) create planar triangles. Then we construct a dual co-volume grid on such triangulation, i.e. at each node X_i we create a finite volume V_i bounded by straight lines that connect midpoints between X_i and its neighbours with centres of masses of all planar triangles joined in the node X_i (Fig. 2).

Integrating Eq. (2) over the co-volume V_i and applying Green's theorem we obtain the integral equation

$$\int_{V_i} \frac{\partial u}{\partial t} dx - \int_{\partial V_i} \nabla_S u \cdot \bar{\eta}_i ds = 0, \tag{3}$$

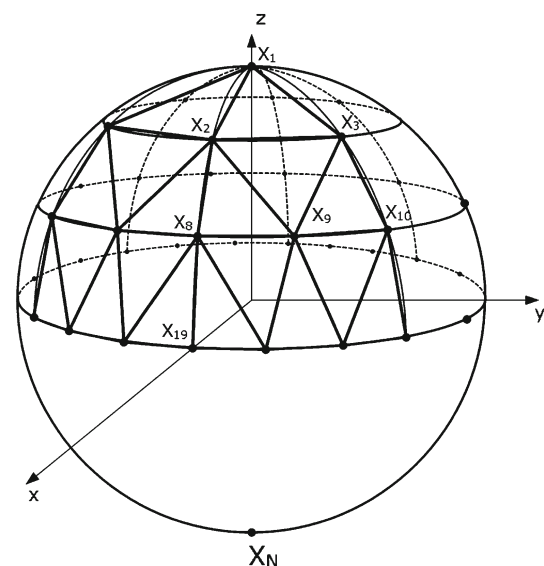


Fig. 1 An example of the triangulation of a sphere with the nodes X_i

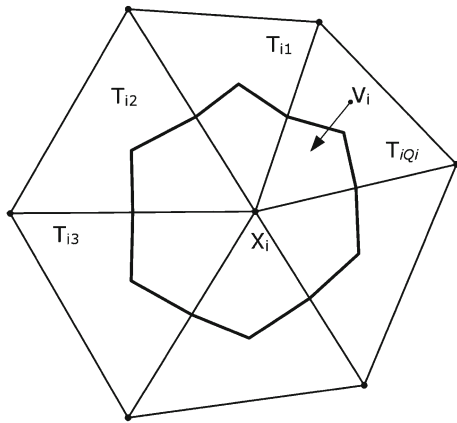


Fig. 2 The co-volume V_i corresponding to the node X_i and the triangles T_{iq} joined at this node

where ∂V_i is the co-volume's boundary and $\bar{\eta}_i$ is the unit outward normal to this boundary considered in the tangential plane to V_i . Taking into account geometry of the co-volume V_i we get the form

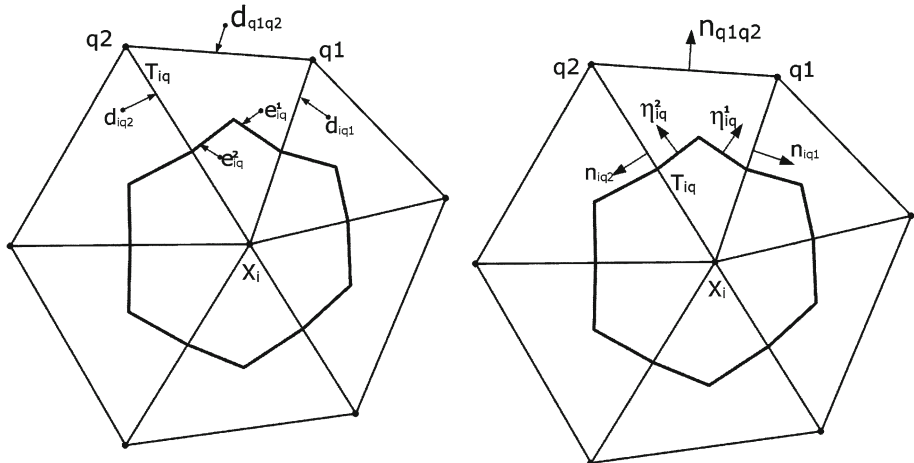
$$\int_{V_i} \frac{\partial u}{\partial t} dx - \sum_{q=1}^{Q_i} \int_{\partial V_{iq}} \nabla_S u \cdot \bar{\eta}_{iq} ds = 0, \tag{4}$$

where ∂V_{iq} are portions of the co-volume's boundary with their normal vectors $\bar{\eta}_{iq}$ (Fig. 3) and Q_i is the number of all triangles joined in the node X_i . This form represents a weak formulation of the problem defined on the finite volume and provides a basis of our SFVM.

In our numerical scheme we consider a piece-wise linear representation of a solution in space and the backward Euler time discretization. Hence, the time derivative is approximated by the backward difference

$$\frac{\partial u}{\partial t} \approx \frac{u^k - u^{k-1}}{\tau}, \quad k = 1, \dots, K \tag{5}$$

Fig. 3 Denotations of the sides of the triangle T_{iq} ($d_{iq1}, d_{iq2}, d_{q1q2}$) and portions of the co-volume's boundary (e_{iq}^1, e_{iq}^2) (left), and the corresponding outward unit normal vectors to the triangle T_{iq} ($n_{iq1}, n_{iq2}, n_{q1q2}$) and to the co-volume's boundary (η_{iq}^1, η_{iq}^2) (right)



where u^k represents the numerical solution in the k th time step and τ is the equidistant discrete time step. Then the first integral in the weak formulation (4) can be replaced by

$$\int_{V_i} \frac{\partial u}{\partial t} dx \approx m(V_i) \frac{u^k - u^{k-1}}{\tau}, \tag{6}$$

where $m(\cdot)$ represents a measure of a given set, in this case the area of the co-volume V_i .

Since we use a linear representation of the solution u^k on each triangle, the surface gradient $\nabla_S u^k$ is constant over each triangle T_{iq} , and we can state

$$\nabla_S u^k \approx P_{T_{iq}}^k = \frac{1}{m(T_{iq})} \int_{T_{iq}} \nabla_S u^k dx. \tag{7}$$

Applying Green's theorem to Eq. (7) we obtain

$$P_{T_{iq}}^k = \frac{1}{m(T_{iq})} \int_{\partial T_{iq}} u^k \bar{n}_{iq} ds, \tag{8}$$

where \bar{n}_{iq} is the unit outward normal to the boundary of the triangle T_{iq} . Taking into account the linear approximation of the solution, the surface gradient can be expressed by a combination of nodal values u_i^k of the approximate solution and by geometry of the triangle T_{iq}

$$P_{T_{iq}}^k = \frac{1}{m(T_{iq})} \left(\frac{u_i^k + u_{q1}^k}{2} d_{iq1} \bar{n}_{iq1} + \frac{u_i^k + u_{q2}^k}{2} d_{iq2} \bar{n}_{iq2} + \frac{u_{q1}^k + u_{q2}^k}{2} d_{q1q2} \bar{n}_{q1q2} \right). \tag{9}$$

Here nodal values of the solution, sizes of the triangular sides and their normal vectors are denoted according to Fig. 3.

Afterwards, an approximation of the weak formulation (4) for the co-volume V_i in the time step k can be written in the form

$$m(V_i) \frac{u_i^k - u_i^{k-1}}{\tau} - \sum_{q=1}^{Q_i} \int_{\partial V_{iq}} P_{T_{iq}}^k \cdot \bar{\eta}_{iq} ds = 0. \tag{10}$$

Since the surface gradient $P_{T_{iq}}^k$ is constant on each triangle and the normal vectors $\bar{\eta}_{iq}$ are constant on each portion ∂V_{iq} of the co-volume's boundary in the triangle T_{iq} , we can rewrite Eq. (10) into the following way

$$m(V_i) \frac{u_i^k - u_i^{k-1}}{\tau} - \sum_{q=1}^{Q_i} \left(m(e_{iq}^1) \bar{\eta}_{iq}^1 \cdot P_{T_{iq}}^k + m(e_{iq}^2) \bar{\eta}_{iq}^2 \cdot P_{T_{iq}}^k \right) = 0, \tag{11}$$

where $m(e_{iq}^1)$ and $m(e_{iq}^2)$ are sizes of the portions of the co-volume's boundary ∂V_{iq} that belong to the same triangle T_{iq} (Fig. 3). Putting known nodal values u_i^{k-1} of the solution from the previous time step to the right-hand-side, we get the final form

$$u_i^k - \frac{\tau}{m(V_i)} \sum_{q=1}^{Q_i} \left(m(e_{iq}^1) \bar{\eta}_{iq}^1 \cdot P_{T_{iq}}^k + m(e_{iq}^2) \bar{\eta}_{iq}^2 \cdot P_{T_{iq}}^k \right) = u_i^{k-1}, \quad \forall i, \tag{12}$$

which represents an implicit numerical scheme for the linear diffusion on a closed surface. Equation (12) is valid for each finite volume V_i , i.e. for $i = 1 \dots, N$, where N is a number of all nodes. It means that Eq. (12) represent a linear system of equations that needs to be computed in every time step

$$\mathbf{A} \mathbf{u}^k = \mathbf{u}^{k-1}, \tag{13}$$

where \mathbf{A} represents the system matrix and $\mathbf{u}^k = \{u_1^k, u_2^k, \dots, u_N^k\}^T$ is the vector of nodal values of the solution in the k th time step. The system matrix \mathbf{A} is the sparse non-symmetrical matrix. Number and locations of non-zero coefficients in the i th row of the matrix \mathbf{A} depends on the number of neighbours of the particular node X_i , and on numbering of the nodes for a chosen triangulation. An appropriate choice of the time step τ makes the system matrix \mathbf{A} diagonally dominant (see Sect. 5.1). Let us remind that in case of filtering on a closed surface there is no need of a boundary condition.

4 The nonlinear diffusion on a closed surface

In general, the linear diffusion corresponds to the Gaussian filtering (cf. Witkin 1983; Koenderink 1984) which has a uniform smoothing effect. Therefore we extend the surface linear diffusion described by Eq. (2) to a nonlinear diffusion on a surface. A key idea is that the diffusivity coefficient λ in Eq. (1) should be non-uniform and dependent on a solution. In our approach we use an analogy to the regularized Perona–Malik model (Catté et al. 1992) applied to the filtering on a

closed surface, i.e. we use the regularized surface Perona–Malik model in the form

$$\frac{\partial u}{\partial t} - \nabla_S \cdot (g(|\nabla_S u^\sigma|) \nabla_S u) = 0, \tag{14}$$

which represents the nonlinear parabolic PDE. Here the function g is the edge detector defined as

$$g(|\nabla_S u^\sigma|) = \frac{1}{1 + H |\nabla_S u^\sigma|^2}, \tag{15}$$

where u^σ is the solution of the linear diffusion obtained for a short time step σ and $H > 0$ is a parameter that gives us a decision capability which gradients preserve. Hence, the edge detector depends on surface gradients of the solution, i.e. large gradients yield its small values and opposite. Such nonlinearity allows adaptive smoothing. An appropriate choice of the parameter H plays an important role in the filtering process and needs to be tuned experimentally.

In order to approximate numerically the surface nonlinear diffusion equation (14), we again apply SFVM. In the following equations we use the same denotations as described in Sect. 3. Integrating Eq. (14) over the co-volume V_i ,

$$\int_{V_i} \frac{\partial u}{\partial t} dx - \int_{V_i} \nabla_S \cdot (g(|\nabla_S u^\sigma|) \nabla_S u) dx = 0, \tag{16}$$

and applying Green's theorem to the second integral we get a weak formulation of the nonlinear PDE (14) in the form

$$\int_{V_i} \frac{\partial u}{\partial t} dx - \int_{\partial V_i} g(|\nabla_S u^\sigma|) \nabla_S u \cdot \bar{\eta}_i ds = 0. \tag{17}$$

After analogous steps as described in Sect. 3 we obtain

$$m(V_i) \frac{u_i^k - u_i^{k-1}}{\tau} - \sum_{q=1}^{Q_i} \int_{\partial V_{iq}} g(|P_{T_{iq}}^{\sigma, k-1}|) P_{T_{iq}}^k \cdot \bar{\eta}_{iq} ds = 0, \tag{18}$$

and finally the form

$$m(V_i) \frac{u_i^k - u_i^{k-1}}{\tau} - \sum_{q=1}^{Q_i} \left(m(e_{iq}^1) \bar{\eta}_{iq}^1 \cdot P_{T_{iq}}^k g(|P_{T_{iq}}^{\sigma, k-1}|) + m(e_{iq}^2) \bar{\eta}_{iq}^2 \cdot P_{T_{iq}}^k g(|P_{T_{iq}}^{\sigma, k-1}|) \right) = 0, \tag{19}$$

which represents a semi-implicit numerical scheme for the nonlinear diffusion on a closed surface. Here the edge detector depends on $P_{T_{iq}}^{\sigma, k-1}$, i.e. on the surface gradients of the solution obtained from the previous time step, which is slightly smoothed by the linear diffusion using one implicit time step with the length σ .

Comparing the semi-implicit scheme in Eq. (19) with the implicit scheme for the linear diffusion in Eq. (12), the only

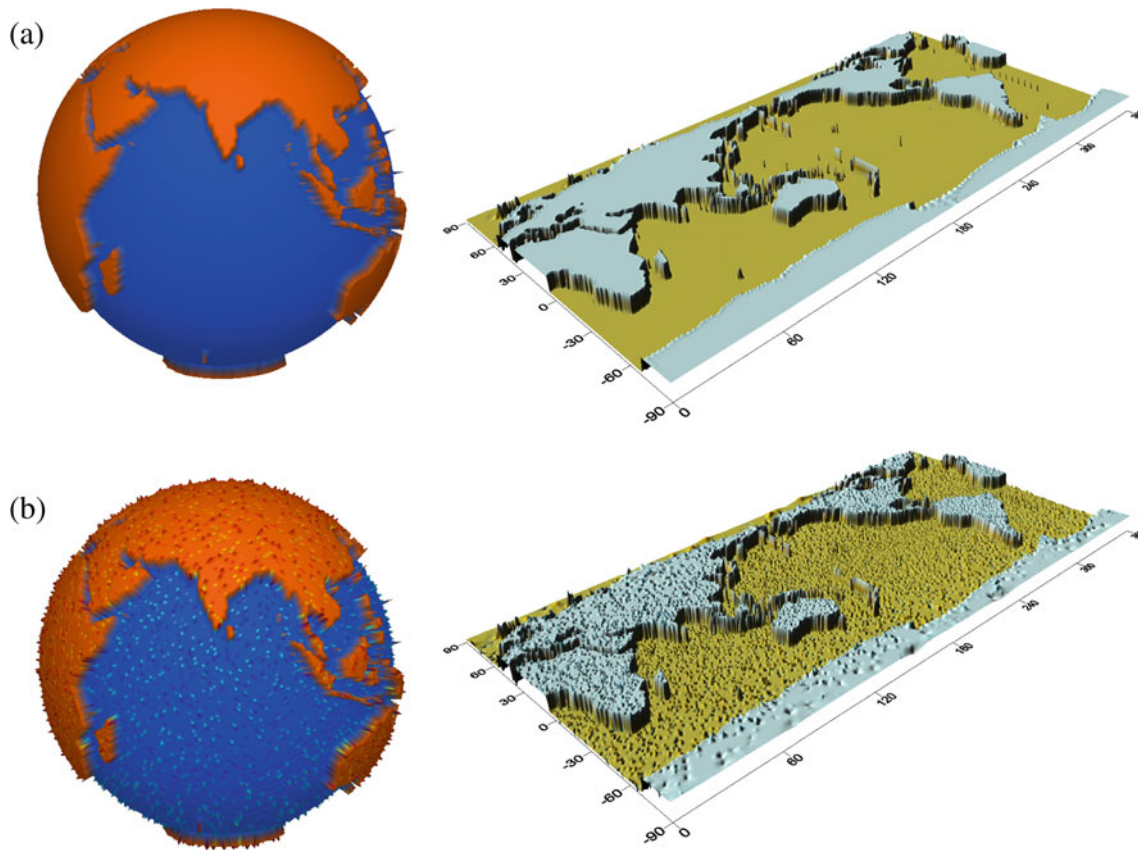


Fig. 4 **a** The artificial function u defined on a sphere which equals to 1 on lands and to 0 at oceans, **b** the function u with the uniform additive noise up to 40 % at 10 % of all nodes

difference is that now the surface gradients $P_{T_{iq}}^k$ are multiplied by the edge detector. This allows an adaptive smoothing according to surface gradients of the solution obtained from the previous time step. Consequently, the edge detector is step by step evolving in time giving an opportunity to preserve main structures and effectively reduce the noise.

5 Numerical experiments

We present four numerical experiments. The first one has an illustrative character showing how an additive noise is filtered out from an artificial function defined on a sphere. In this experiment an exact solution is known therefore we are able to demonstrate an efficiency of our filtering methods using quantitative measures. SD of residuals between the exact and filtered solutions for different parameters and iterative steps are our indicator in the process of tuning optimal parameters for the edge detector.

Other three examples deal with filtering of the real geodetic data on the Earth's surface, namely (i) we reduce a stripping noise from the GOCE satellite only geopotential model up to degree 240, (ii) we filter noise from the real GOCE measurements, namely the component T_{zz} , and (iii)

we reduce a stripping noise from the satellite only mean dynamic topography (MDT) at oceans. In all experiments we focus on a comparison of the results obtained by both the linear and nonlinear models presenting advantages of the nonlinear diffusion.

5.1 Filtering of the additive noise

In the first numerical experiment we test our linear and nonlinear diffusion filtering on a sphere reducing an additive noise. At first we approximate the sphere by a triangulation that is based on a subsequent division of a 12-hedron (Fig. 1) using the same strategy as described in Čunderlík et al. (2008). In this experiment we use the triangulation with 102,402 nodes that corresponds to the resolution of 0.5625° in latitude.

On this triangulated sphere we define an artificial function u in such a way that $u_i = 1$ for all nodes located on lands and $u_i = 0$ for all nodes at oceans (Fig. 4a). On this function we put a uniform additive noise up to 40 % at 10 % of all nodes randomly distributed over the globe (Fig. 4b), i.e. the generated uniform non-Gaussian additive noise is from the interval $(-0.4, 0.4)$ and its SD is 0.232. After that $u_i \in (0.6, 1.4)$ on

lands and $u_i \in (-0.4, 0.4)$ at oceans. Such data represent our initial condition u^0 . Our goal is to reconstruct the original function u using the proposed SFVM numerical schemes.

In case of the linear surface diffusion, the linear system of equations is given by the implicit numerical scheme in Eq. (12) and needs to be computed in every filtering time step. In our experiments we use the iterative successive over-relaxation (SOR) method (Barrett et al. 1994). In order to get a stability and convergence of SOR, we make the system matrix \mathbf{A} diagonally dominant choosing the time step τ proportional to an average area of the co-volumes

$$\tau \approx \frac{1}{N} \sum_{i=1}^N m(V_i). \tag{20}$$

Such a coupling is natural for solving the parabolic PDEs also due to precision reasons (Dziuk and Elliott 2007). The choice of the time step is essential for the whole filtering process and implies how many filtering steps (or iterations) will be necessary to get reasonable results. (Remark: to distinguish between terms, a number of filtering steps corresponds to a number of time steps used for solving the linear or nonlinear diffusion equation, and the time step τ in a discretization of PDE can be called in this application “the discrete filtering step”). For simplicity, in the following we use the term “number of iterations” instead of “number of filtering steps”, since such terminology is standard in diffusion filtering). Our numerical results obtained after 10, 20, 40 and 100 iterations of the linear diffusion filtering ($\tau = 10^9$) are depicted in Fig. 6a (left). Figure 7a shows the corresponding profiles along the equator across Africa.

In case of the nonlinear surface diffusion, the linear system of equations is given by the semi-implicit numerical scheme in Eq. (19). To get this system, first we have to apply the linear diffusion filtering for the solution in the previous time step for a short time step σ . Then we evaluate the corresponding surface gradients that indicate values of the edge detector. After that we are able to compute non-zero coefficients of the system matrix. This process is repeated in every iteration (filtering step). Therefore, the nonlinear surface diffusion filtering is more time consuming and usually requires more iterations.

Here the crucial part is to find optimal parameters for the edge detector. Since in this experiment we know the exact solution, we are able to tune them considering the SD of residuals between the exact and filtered solutions for different parameters and iterative steps. Graphs in Fig. 5 show which parameters give the best results for the chosen time step $\tau = 10^9$. They also demonstrate how the choice of the parameters H and σ (compare Fig. 5a, b) can influence the quality of results as well as a number of iterations necessary to reach satisfactory results.

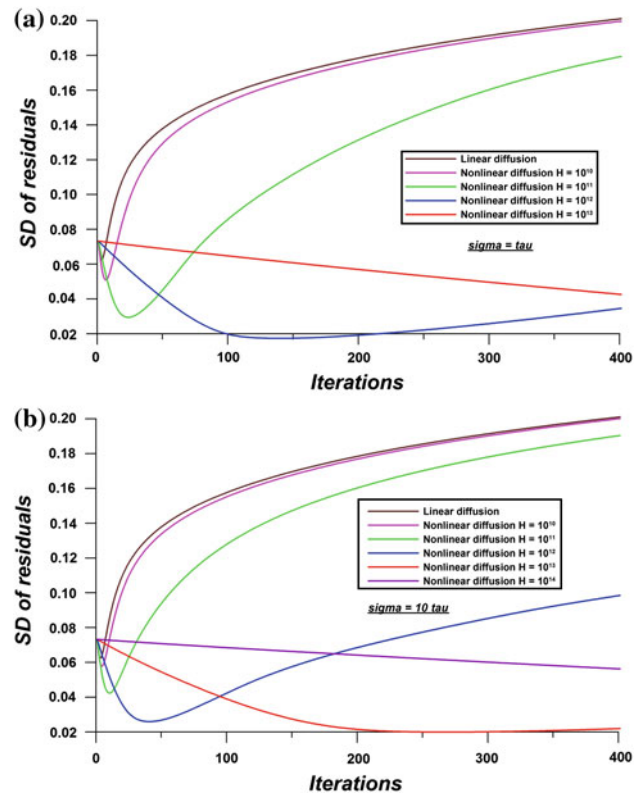


Fig. 5 Filtering of the additive noise: SD of residuals between the exact and filtered solutions using the linear and nonlinear surface diffusion with different parameters of the edge detector ($\tau = 10^9$) **a** $\sigma = \tau$, **b** $\sigma = 10\tau$

Figure 6b depicts the filtered solutions obtained after 25, 50, 100 and 150 iterations of the nonlinear diffusion filtering ($\tau = 10^9, H = 10^{12}, \sigma = \tau$). Figure 7b shows the corresponding profiles along the equator across Africa and Fig. 8 the edge detector for the corresponding time steps. One can see how the edge detector is stepwise evolving in time. The signal corresponding to the additive noise is step by step vanishing while high gradients and their positions remain preserved. Here we remind that the edge detector always depends on surface gradients computed from the solution in the previous iterative step, thus it is adaptive to the filtered solution evolving in time. Such an adaptive smoothing effect is a main advantage of the nonlinear filtering.

Comparing results from the linear and nonlinear filtering (Figs. 6, 7) it is evident that both approaches effectively reduce the additive noise. However, the linear filtering also smooths the main structures, i.e. high gradients on edges of continents, while the nonlinear model preserves them almost unchanged. Considering the SD of residuals between the exact and filtered solutions (Fig. 5), blurring of edges by the linear diffusion yield consistent worsening (after slight improvement at the beginning from 0.073 to 0.062). In contrary, the nonlinear diffusion is able to

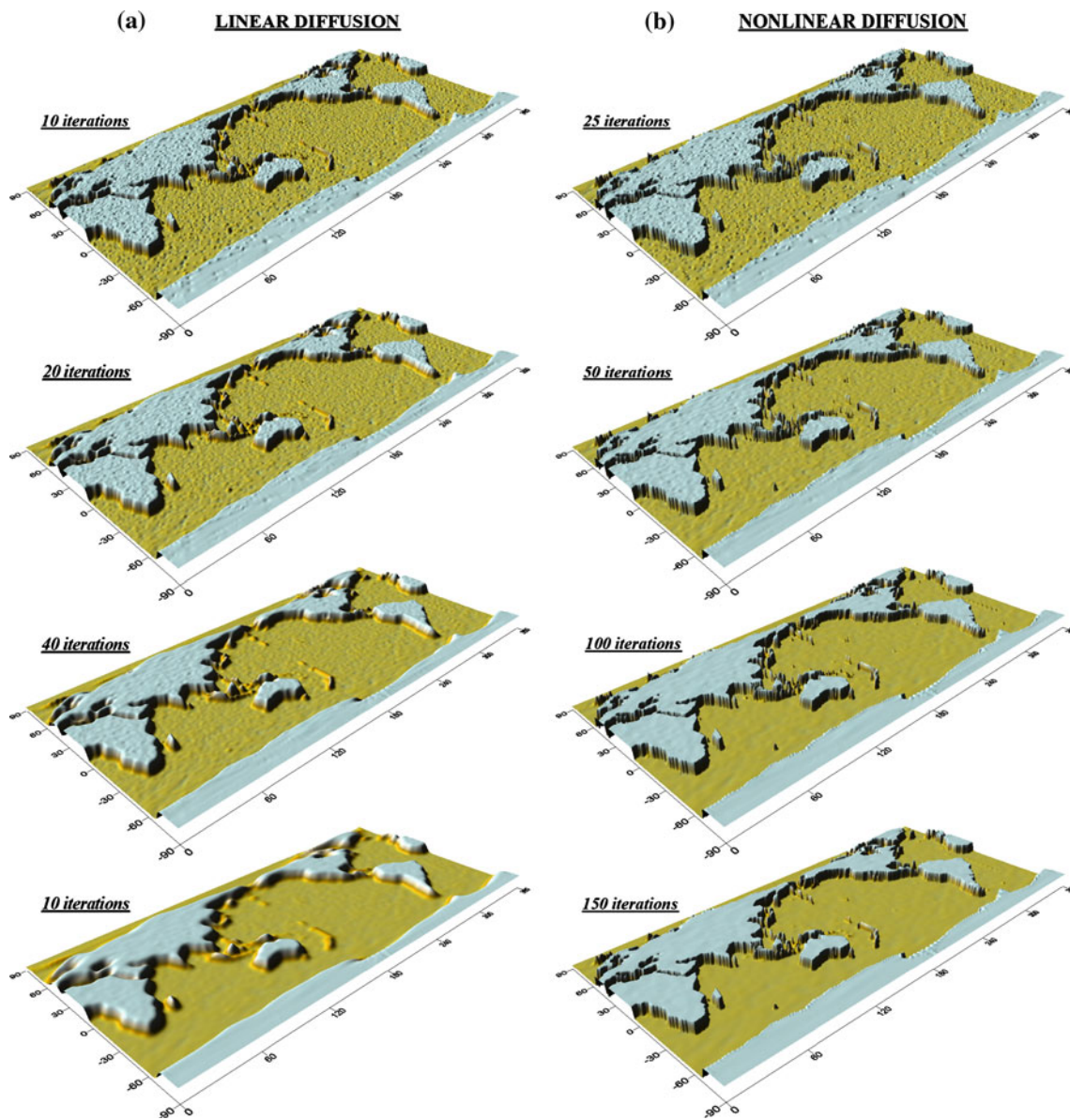


Fig. 6 Filtering of the additive noise using **a** the linear surface diffusion ($\tau = 10^9$), and **b** the nonlinear surface diffusion ($\tau = 10^9$, $H = 10^{12}$, $\sigma = \tau$)

reduce the SD of residuals from 0.073 to 0.017 (an improvement about 77 %) if the optimal parameters of the edge detector are used.

5.2 Filtering of the stripping noise from the GOCE geopotential model

In the second numerical experiment we apply the linear and nonlinear surface diffusion filtering to reduce a stripping noise from the satellite only geopotential models due to a truncation error of the spherical harmonics approach. Namely, we are filtering the disturbing potential evaluated from the second release of the GOCE direct solution

(Bruinsma et al. 2010) up to degree 240 (Fig. 9a). In order to treat better the stripping effect related mostly to higher degree coefficients, our initial conditions u^0 are given by the residual disturbing potential computed from the coefficients between degrees 21 and 240 (Fig. 9b), i.e. we remove the low-frequency part up to degree 20.

In this experiment we use the same level of discretization of the Earth's surface as in the previous experiment, i.e. 102,402 nodes and the resolution 0.5625° in latitude. Since here an exact solution is unknown, we tune optimal parameters for the edge detector comparing our filtered solutions with the residual disturbing potential evaluated from EGM-2008 up to degree 2160 (Pavlis et al. 2008) removing the same

Fig. 7 Profiles along equator across Africa—filtering of the additive noise using **a** the linear surface diffusion, **b** the nonlinear surface diffusion (*blue lines* noisy signal, *red lines* filtered solutions)

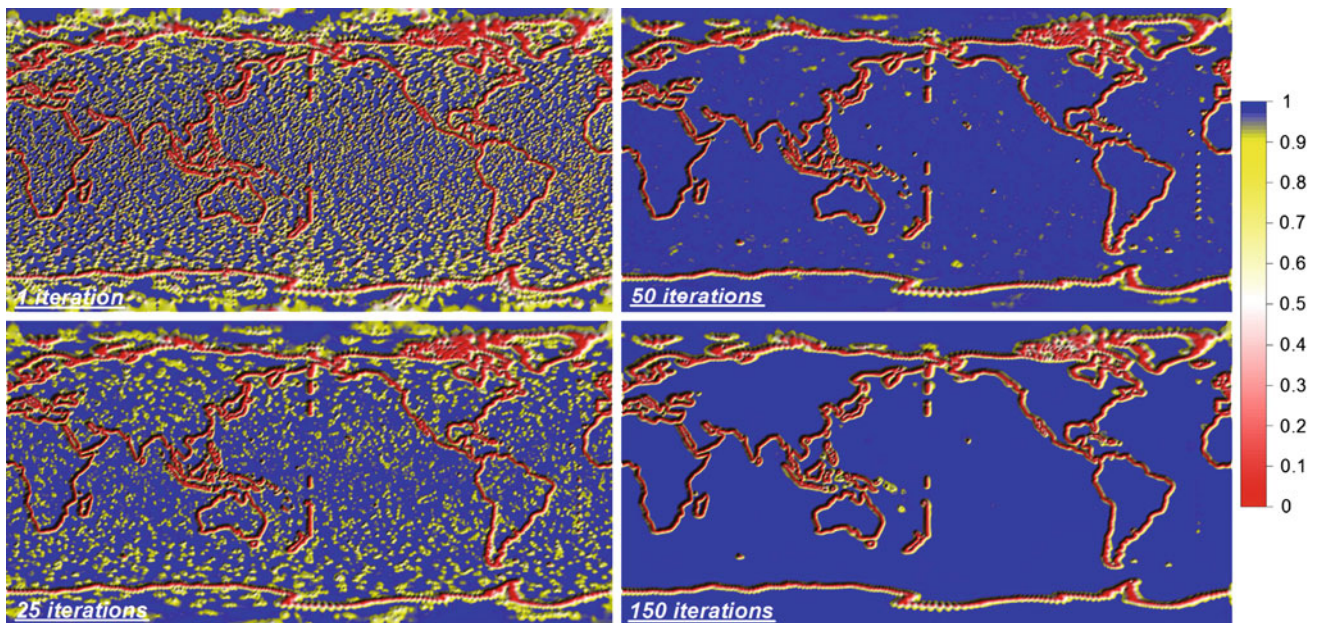
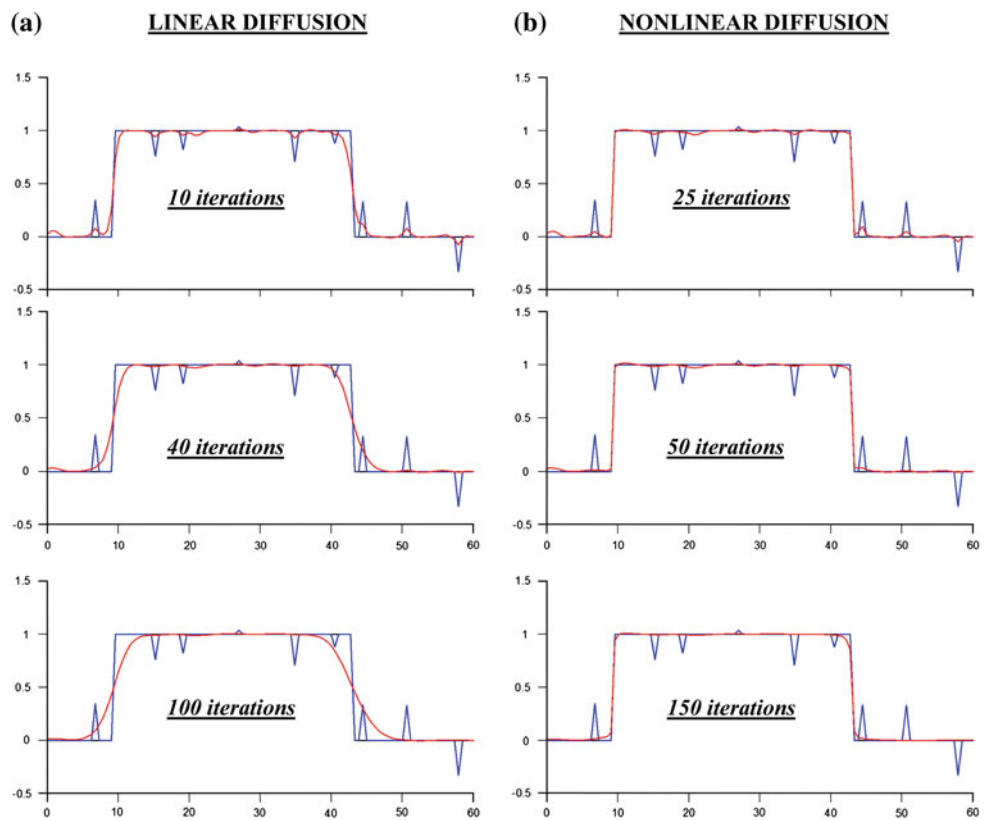
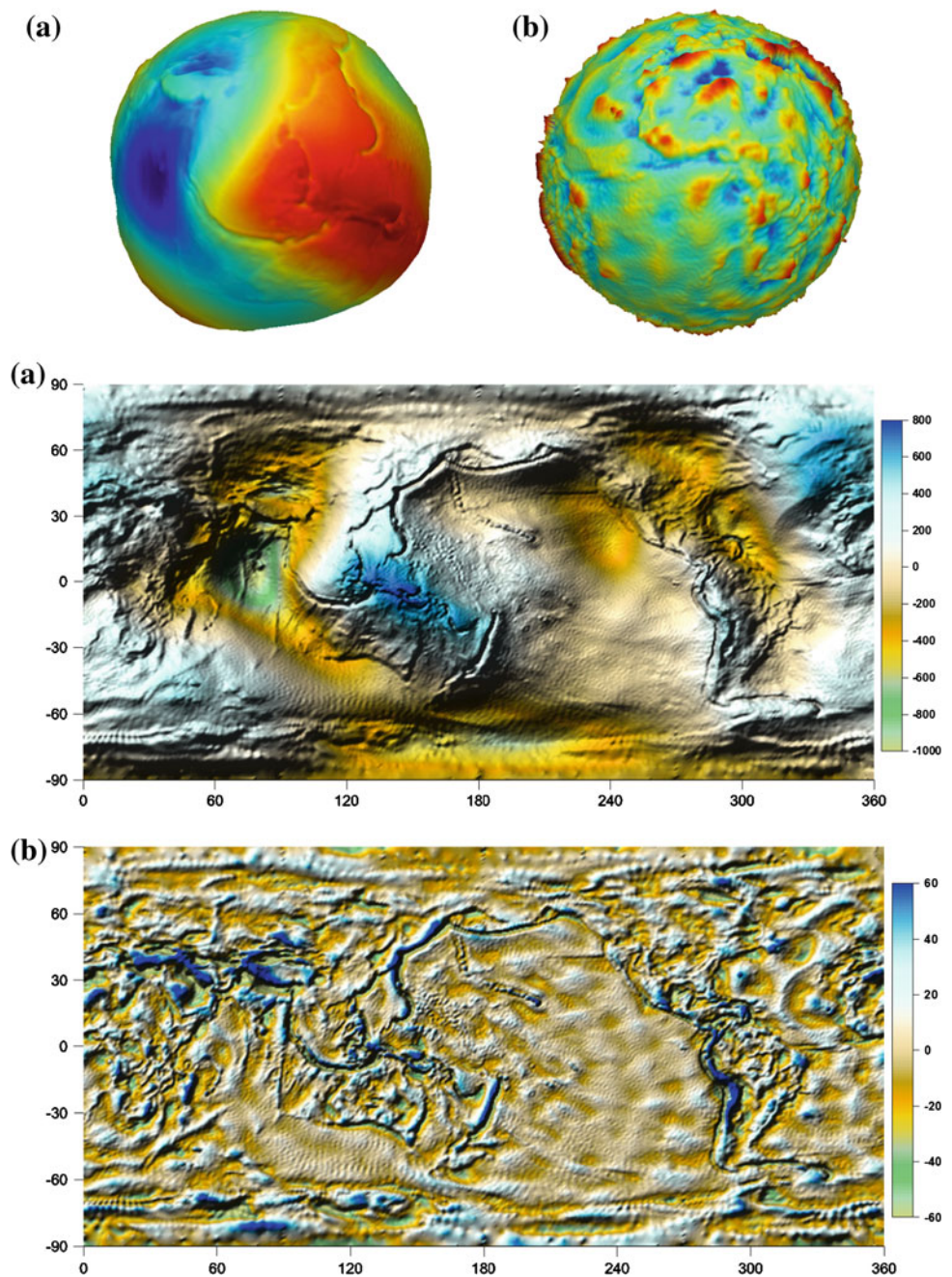


Fig. 8 Edge detector for the nonlinear surface diffusion filtering of the additive noise evolving in time

low-frequency part as in case of our initial data. Our criterion is the SD of residuals at oceans (Fig. 11) supposing that the solution from EGM-2008 is more precise, much smoother and closer to reality. We neglect the fact that both datasets correspond to different time period of input data, which is not

relevant for our purpose to filter out the stripping noise. We omit the residuals on lands due to higher differences especially in mountainous regions. Figure 11 shows that using the parameters $\tau = 10^9$, $H = 10^8$ and $\sigma = \tau$, we get the results, which fit the best to EGM-2008. In this case the SD of the

Fig. 9 **a** The disturbing potential from the second release of the GOCE direct solution up to degree 240, **b** the residual disturbing potential after removing the low-frequency part up to degree 20 (unit: $\text{m}^2 \text{s}^{-2}$)



residuals at oceans is reduced from 3.526 to $3.266 \text{ m}^2 \text{ s}^{-2}$ (an improvement about 7 %). In the case of the linear diffusion an improvement is much smaller, i.e. about 2 % (from 3.526 to $3.459 \text{ m}^2 \text{ s}^{-2}$).

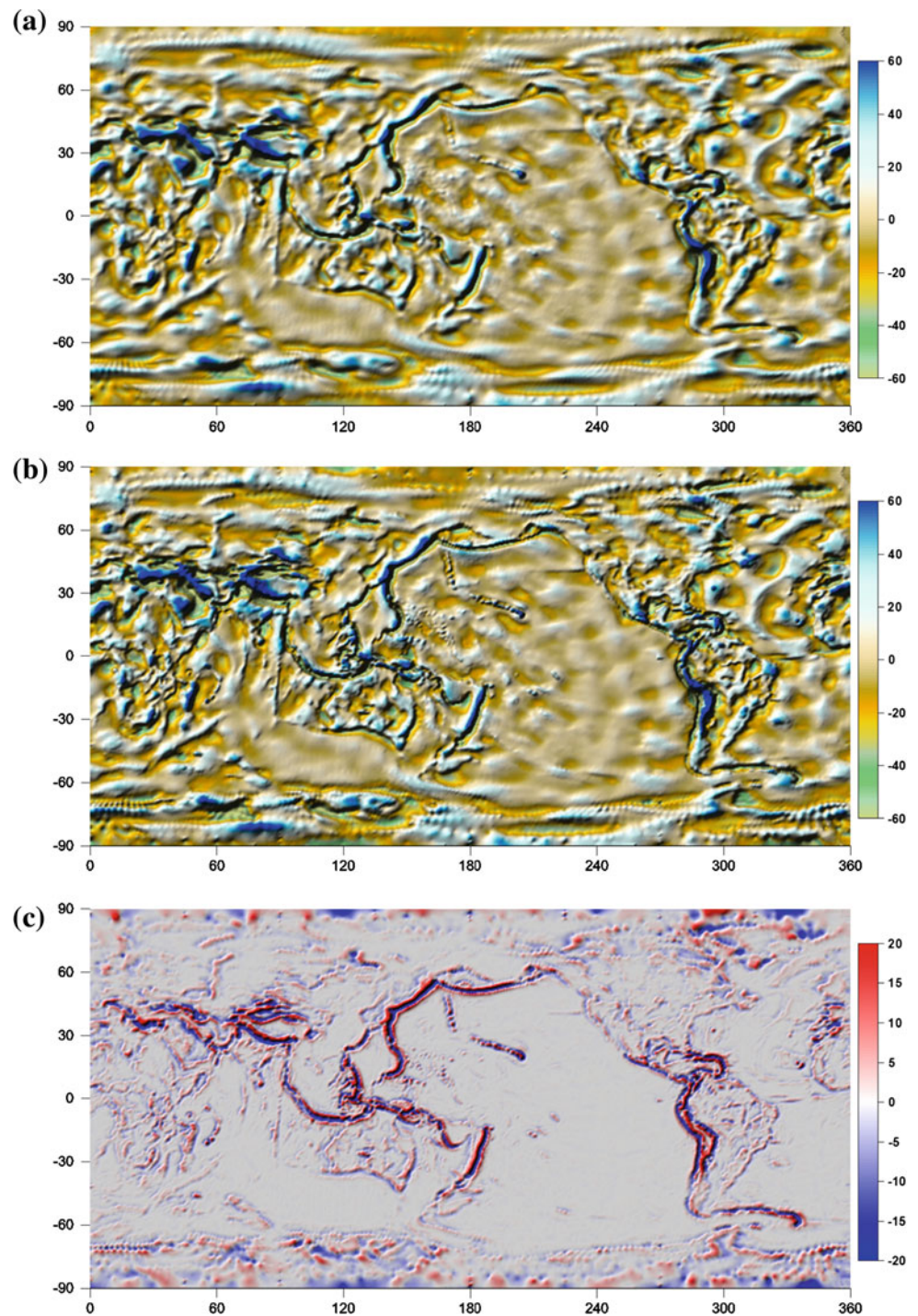
Figure 10a depicts our final solution obtained after 300 iterations of the linear diffusion filtering, Fig. 10b the results after 500 iterations of the nonlinear diffusion filtering and Fig. 10c the residuals between both solutions. Figure 12 shows how the edge detector is evolving in time. One can see how the edge detector is step by step closer to 1 in areas of smaller gradients of the solution, where the stripping noise finally vanishes. In areas of high gradients of the gravity field

the edge detector remains close to 0 and these zones are only slightly smoothed. This is a main advantage in comparison with the linear diffusion filtering whose uniform smoothing effect does not preserve the main structures and smoothes them rapidly (Fig. 10a). Consequently the highest residuals between the linear and nonlinear filtering are in these zones of abrupt changes in the gravity field (Fig. 10c).

5.3 Filtering of the noise from the GOCE measurements

In the third experiment we filter the noise from the real GOCE measurements, namely from the component T_{zz} . We process

Fig. 10 The filtered residual disturbing potential obtained **a** after 300 iterations of the linear diffusion, and **b** after 500 iterations of the nonlinear diffusion filtering, and **c** the residuals between both solutions (unit: $\text{m}^2 \text{s}^{-2}$)



data observed during the period November–December 2009. In this experiment we increase a level of the discretization into the resolution 0.25° (518,402 nodes) in order to capture better a dense coverage of the original GOCE measurements. Artificially generated positions of 518,402 nodes of the regular triangulation are replaced by 3D positions of the nearest neighbour real GOCE measurements. It means the polyhedral approximation of our computational domain is given by 3D positions of the GOCE mission in the time when the

chosen measurements were observed. Missing values in the polar gaps are simulated from the GOCE-DIR2 geopotential model up to degree 240. An altitude of these “polar nodes” is prescribed to 249 km above the reference ellipsoid. In this way we get our computational domain as well as initial data for filtering (Fig. 13a).

In comparison with the previous experiment (Sect. 5.2), smaller sizes of the co-volumes and a different character of the noise have forced us to decrease the iterative time step

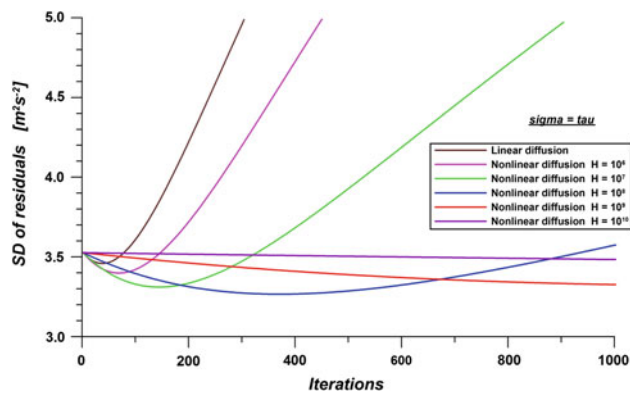


Fig. 11 Filtering of the residual disturbing potential from GOCE-DIR2: SD of residuals at oceans between the filtered solutions and EGM-2008 using the linear and nonlinear surface diffusion with different parameters of the edge detector ($\tau = 10^9$)

to $\tau = 10^8$. The optimal parameters of the edge detector were tuned experimentally ($H = 10^{12}$ and $\sigma = \tau$). Figure 13 depicts the obtained results after 10 and 30 iterations of the linear (Fig. 13b) as well as nonlinear diffusion filtering (Fig. 13c). For a better visualization of the noise in Fig. 13a–c, the signal of T_{zz} simulated from GOCE-DIR2 up to degree 240 is removed. Figure 13d shows a comparison between the linear and nonlinear diffusion filtering after 10 and 30 iterations. One can see how the linear diffusion step by step smoothes also main structures especially in areas of abrupt changes in the gravity field, while the nonlinear diffusion preserves them effectively reducing the noise. In

these zones the linear filtering after 30 iterations can reach a loss of information more than 20 % of the signal (Fig. 13d).

5.4 Filtering of the stripping noise from the satellite only MDT

The last numerical experiment deals with the diffusion filtering of a stripping noise from the satellite only MDT obtained from the CNES_CLS_10 mean sea surface model and the GOCE-DIR2 geoid model up to degree 240 (Fig. 14a). Both models are available from the GOCE User Toolbox (GUT) (ESA 2011). In this experiment we use the same discretization level as in the previous case, i.e. the resolution 0.25° (518,402 nodes), however the nodes are located on the Earth's surface.

In order to find optimal parameters of the edge detector, we compare the filtered solutions with the MDT_CNES_CLS_09 model (available from GUT) (Fig. 14b). Here we have to realize that a final result, i.e. the filtered MDT, is very smooth surface in comparison with amplitudes of the stripping noise. It means we have to find such parameters of the edge detector that will be very sensitive to small gradients of MDT and at the same time will reduce high stripping noise. This can be achieved using the parameter σ much higher than τ . For such purposes we compare our filtering solutions with MDT_CNES_CLS_09. We focus on the residuals in area of the Antarctic Circumpolar Current (ACC) in order to see which parameters preserve better significant gradients of MDT in this zone.

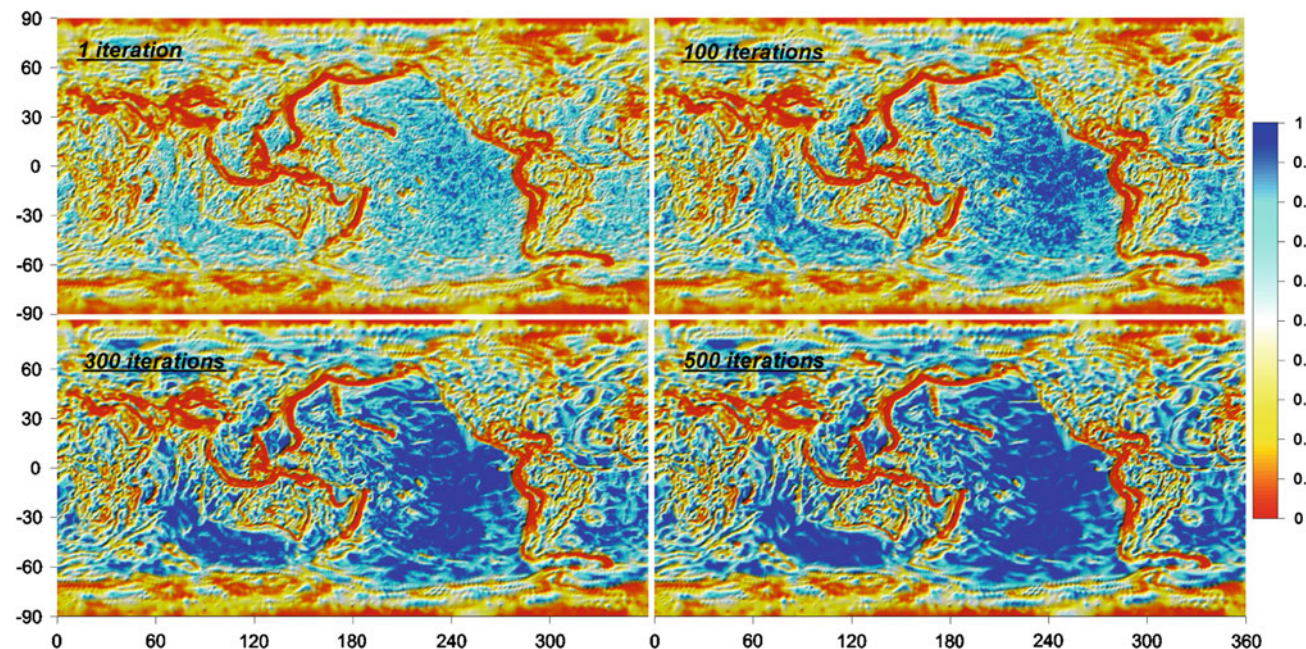


Fig. 12 The edge detector of the nonlinear surface diffusion filtering evolving in time ($\tau = 10^9$, $H = 10^8$, $\sigma = \tau$)

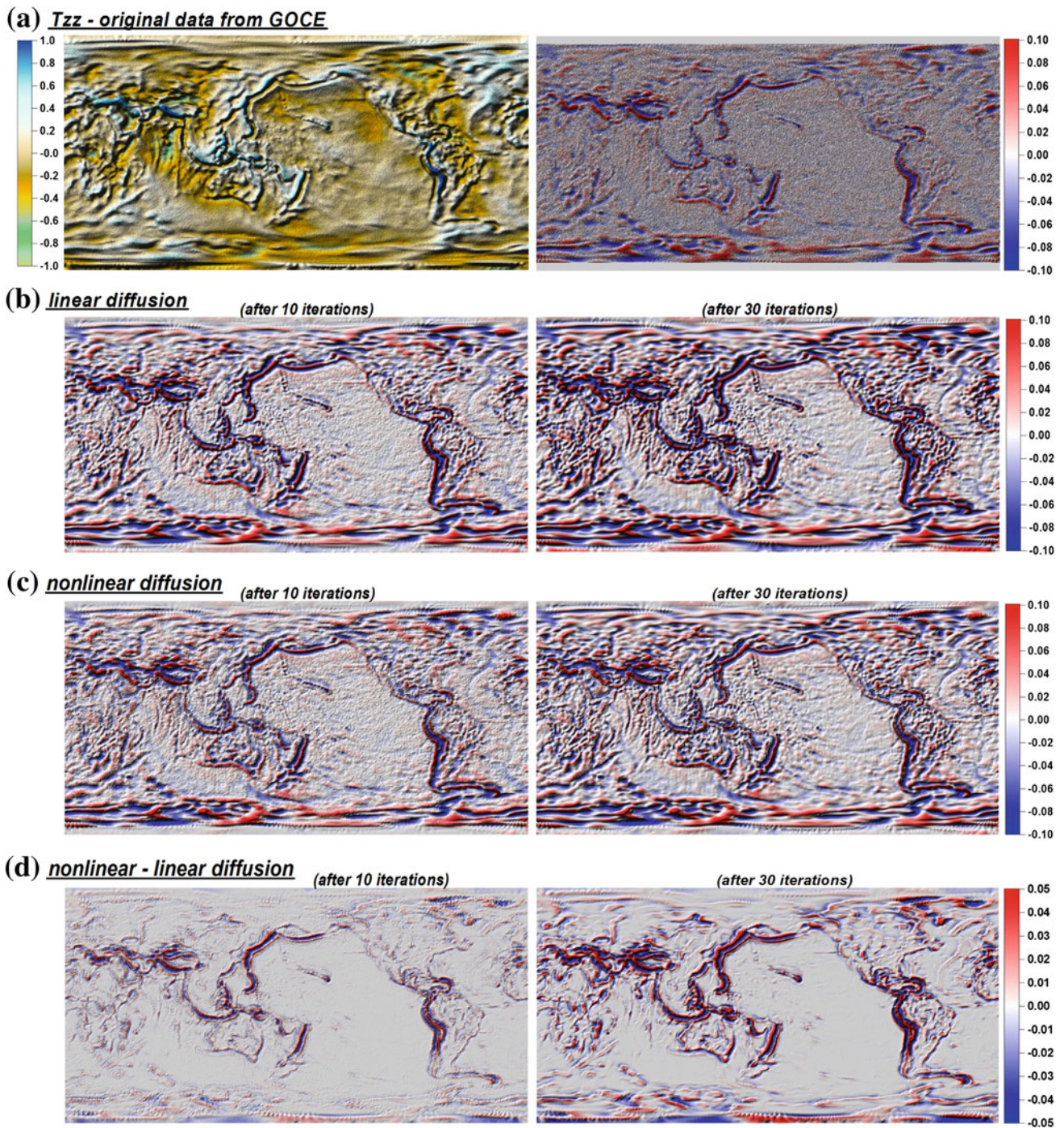


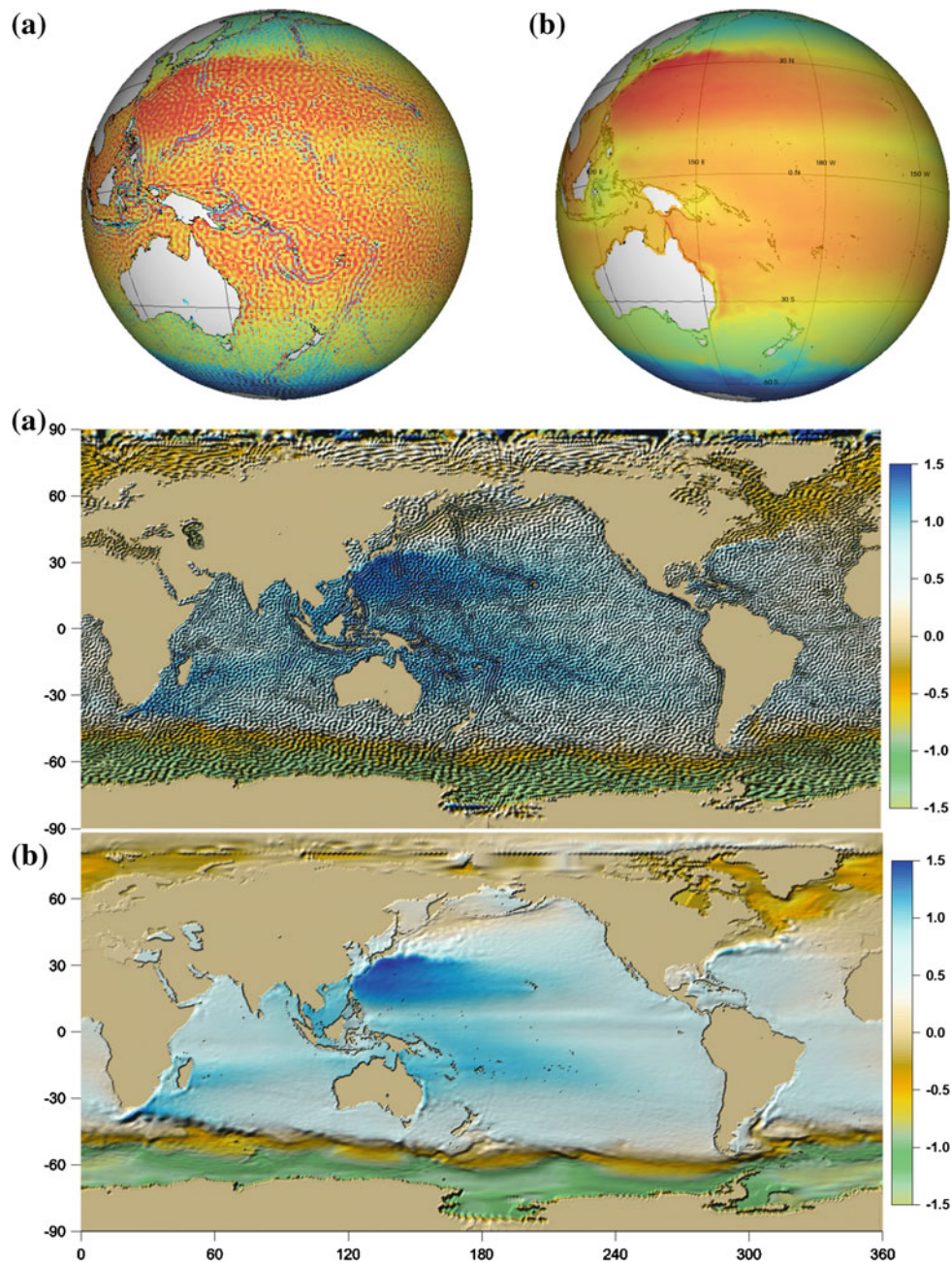
Fig. 13 Filtering of the noise from the real measurements of GOCE, namely the component T_{zz} (a), using the linear diffusion (b), and the nonlinear diffusion (c), and their comparison (d) (unit: Eötvös). For a

better visualization of the noise, the signal simulated from GOCE-DIR2 up to d/o 240 is removed in a right, b and c

Figure 15 depicts graphs of minimal SD of the residuals in area of ACC between the filtered solutions and MDT_CNES_CLS_09 using the different parameter H and ratio (σ/τ) of the edge detector. Such analysis is performed for two different time steps (i) $\tau = 0.5 \times 10^9$ (Fig. 15a), and (ii) $\tau = 1.0 \times 10^9$ (Fig. 15b). Each point of the graph

represents the minimal value of the SD for the specified combination of parameters. The number above this point corresponds to the number of iterations necessary to reach the minimum. For example, in case of $\tau = 0.5 \times 10^9$ (Fig. 15a), the best results are achieved for $H = 10^{12}$, $\sigma = 25\tau$ and using 25 iterations. The similar results can be obtained using

Fig. 14 **a** “Satellite-only” mean dynamic topography model obtained from the CNES_CLS_10 mean sea surface model and the GOCE-DIR2 geoid model up to d/o 240, and **b** the MDT_CNES_CLS_09 model (all models available from the GOCE User Toolbox) (unit: m)



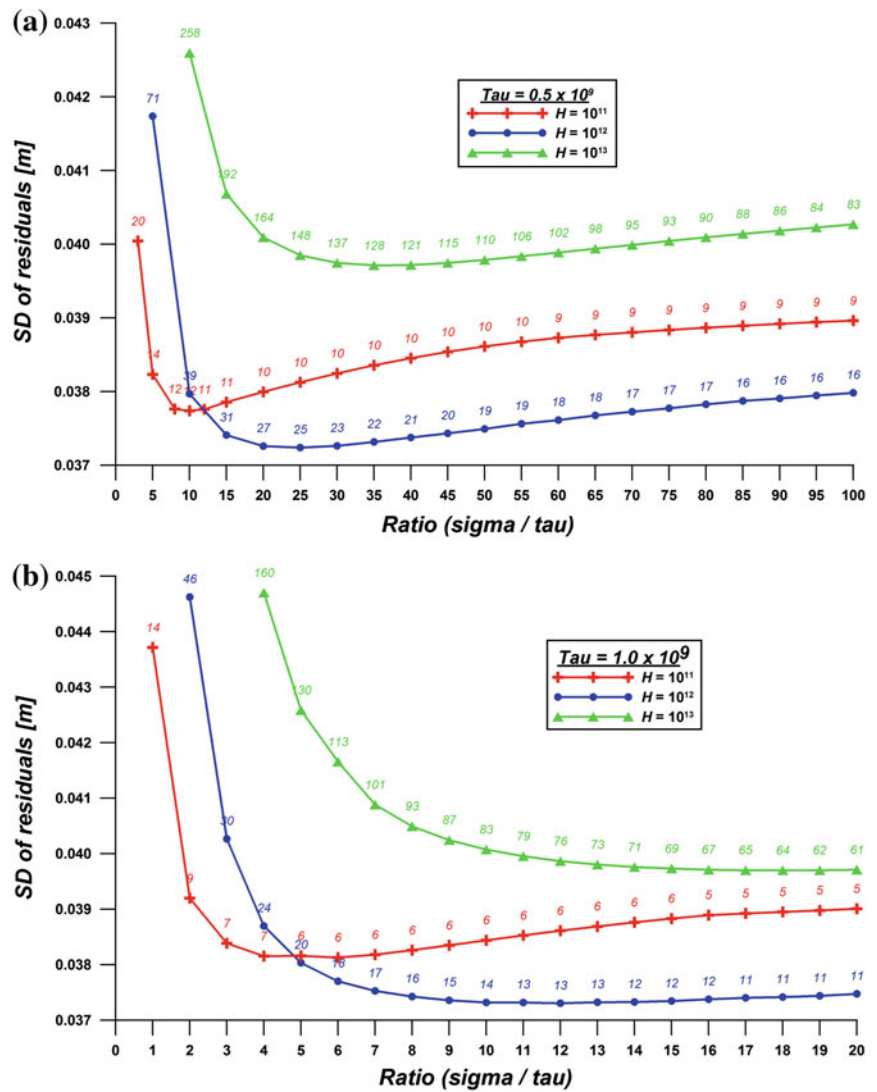
13 iterations and $\tau = 1.0 \times 10^9$, $H = 10^{12}$ and $\sigma = 12\tau$ (Fig. 15b). Anyhow, graphs in Fig. 15 indicate that a combination of the very smooth signal (e.g. MDT) and the relatively high noise requires the parameter σ much higher than τ .

Figure 16 depicts the filtered satellite only MDT after 10 and 25 iterations of the linear (Fig. 16a) as well as nonlinear diffusion filtering (Fig. 16b). Their comparison is depicted in Fig. 16c. It shows how the nonlinear diffusion filtering preserves main gradients in MDT important for oceanographic applications (e.g. in areas of ACC, Kuroshio current and Gulf Stream), while the linear diffusion smooths them significantly. Figure 16d depicts differences between filtered solu-

tions after 25 and 10 iterations. It confirms a fact that too long filtering can slowly smooth also important structures with small amplitudes, e.g. in area of the equatorial currents in the Pacific Ocean.

Finally we use our filtered satellite only MDT as well as the GUT a priori MDT_CNES_CLS_09 and MDT_DTU10 models to compute derived oceanographic characteristics. Figure 17 depicts the zonal velocity component of the ocean geostrophic surface currents. Figure 18 shows the velocity speed of the ocean geostrophic surface currents in area of the Aghulas current. The visual comparison indicates how the preserving of the main gradients in MDT by the nonlinear

Fig. 15 Nonlinear filtering of the satellite-only MDT: minimal SD of the residuals between the filtered solutions and MDT_CNES_CLS_09 using the different parameter H and ratio (σ/τ) of the edge detector, **a** $\tau = 1.0 \times 10^9$, and **b** $\tau = 0.5 \times 10^9$. Each point of the graph represents the minimal value of the SD for the specific parameters. The number above this point corresponds to the number of iterations necessary to reach the minimum (SD are computed only from residuals in area of the Antarctic Circumpolar Current)



filtering is important for oceanographic purposes. This highlights an efficiency of the presented nonlinear diffusion filtering method.

5.5 Computational aspects

All presented computations were performed on a standard PC (2.4 GHz) requiring less than 1 GB of internal memory. Memory requirements as well as the total CPU time depend on a level of the discretization. In the first two numerical experiments with 102,402 nodes (Sects. 5.1 and 5.2), every 100 iterations took about 58 s for the linear and 72 s for the nonlinear diffusion filtering using only 30 MB of the internal memory. In the experiments with 502,402 nodes (Sects. 5.3 and 5.4), every 30 iterations took about 94 s for the linear and 122 s for the nonlinear diffusion filtering using 141 MB. Such relatively small memory requirements give an opportunity to filter data with much higher resolution. For example,

using 4 GB of the internal memory we can reach a level of the discretization with the resolution of 0.05° (3 arc min) corresponding to 12,960,002 nodes.

Besides the level of discretization, the total CPU time is also influenced by a choice of the time step τ and σ . They have essential impact on an overall duration of filtering as well as on properties of the system matrix \mathbf{A} that determine a number of iterations necessary to reach prescribed precision in the SOR iterative method. However, the most time consuming part of the whole process is to find optimal parameters for the nonlinear model that would give the most satisfactory results. It means to tune the parameter H of the edge detector (15) that is highly related to σ , i.e. to the short implicit time step of the linear diffusion that is used to smooth the solution from the previous time step. On the other hand, once the optimal parameters are tuned for a specific type of data, they can be used for different datasets of the same type, e.g. in case of periodical monitoring of some quantity.

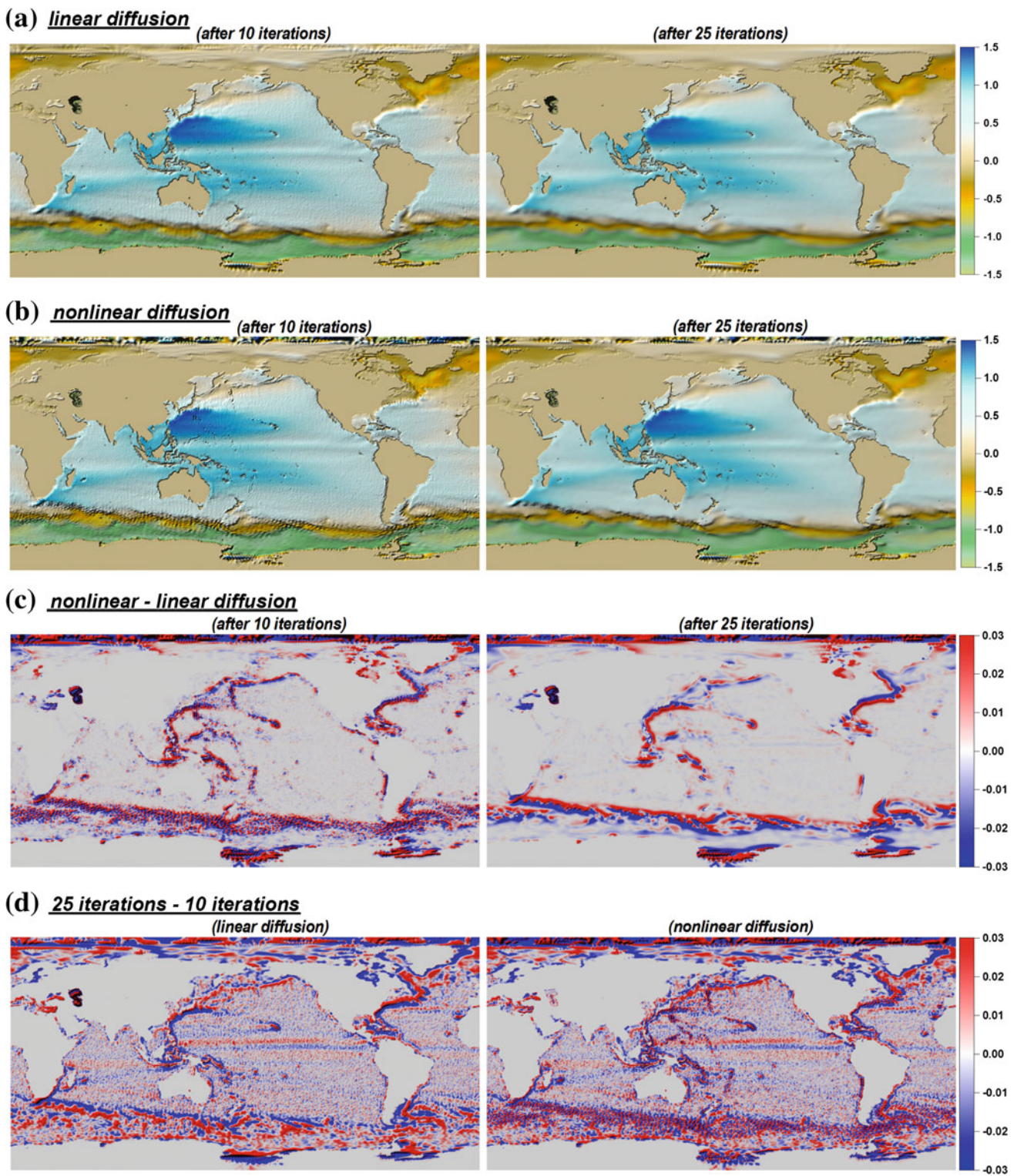


Fig. 16 Filtering of the satellite-only mean dynamic topography (Fig. 14a) using **a** the linear diffusion ($\tau = 0.5 \times 10^9$), **b** the nonlinear diffusion ($\tau = 0.5 \times 10^9$, $H = 10^{12}$, $\sigma = 25\tau$), **c** their comparison, and **d** differences between filtered solutions after 25 and 10 iterations (unit: m)

Finally, the time when to stop filtering plays an important role in the whole process. There are several possible techniques which can be taken into consideration, e.g. to stop

the filtering process if the L2 norm of differences between two consecutive filtering steps is below a specified threshold. However, a theoretical solution how to select an optimal

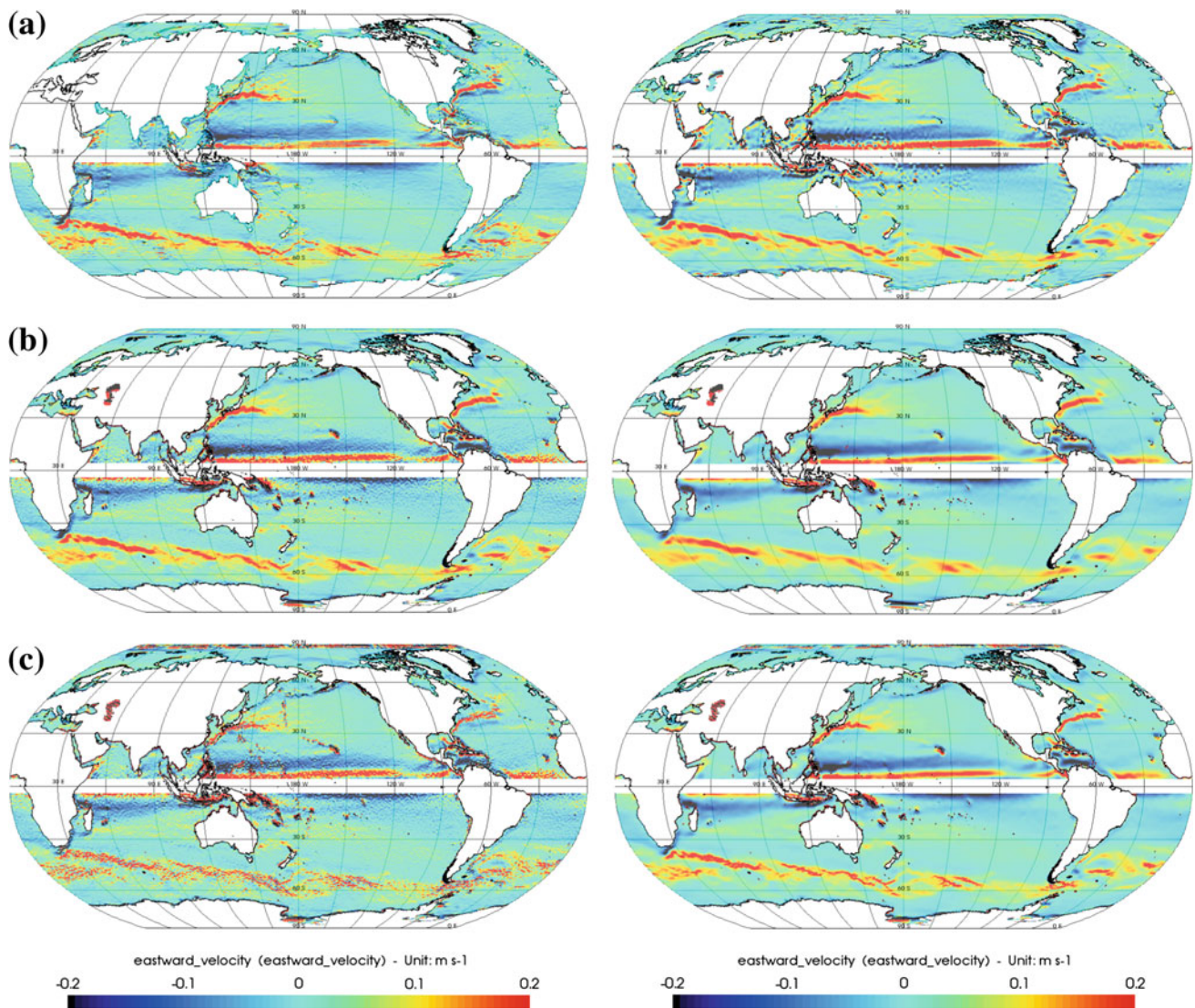


Fig. 17 The zonal velocity component of the ocean geostrophic surface currents computed from **a** the GUT a priori MDT_CNES_CLS_09 (left) and MDT_DTU10 (right), and from the satellite-only MDT fil-

tered using **b** the linear diffusion after 10 (left) and 25 (right) iterations, and **c** the nonlinear diffusion after 10 (left) and 25 (right) iterations

stopping time is still an objective of mathematical investigations (cf. Capuzzo Dolcetta and Ferretti 2001).

6 Discussion and conclusions

The developed filtering methods based on numerical solutions to the linear and nonlinear diffusion equations on close surfaces like a sphere, ellipsoid or the Earth's surface represent an original approach for filtering data in geodesy. The implicit and semi-implicit numerical schemes, derived using the proposed surface finite volume method, are efficient for linear and nonlinear filtering. Numerical experiments show that both linear and nonlinear models can effectively reduce

noise. However, the linear diffusion also smoothes main and important structures or edges in filtered data, while the nonlinear diffusion allows preserving them. This adaptive smoothing effect in comparison with the uniform one of the linear filtering is a principal advantage of the nonlinear filtering.

The presented nonlinear filter based on the regularized surface Perona–Malik model requires tuning optimal parameters of the edge detector for specific data. It means to find the most appropriate combination of the time step τ , the sensitivity parameter H and the short implicit time step σ for linear smoothing of the solution from the previous time step. This is usually the most time consuming part of the whole filtering process. On the other hand it gives users a

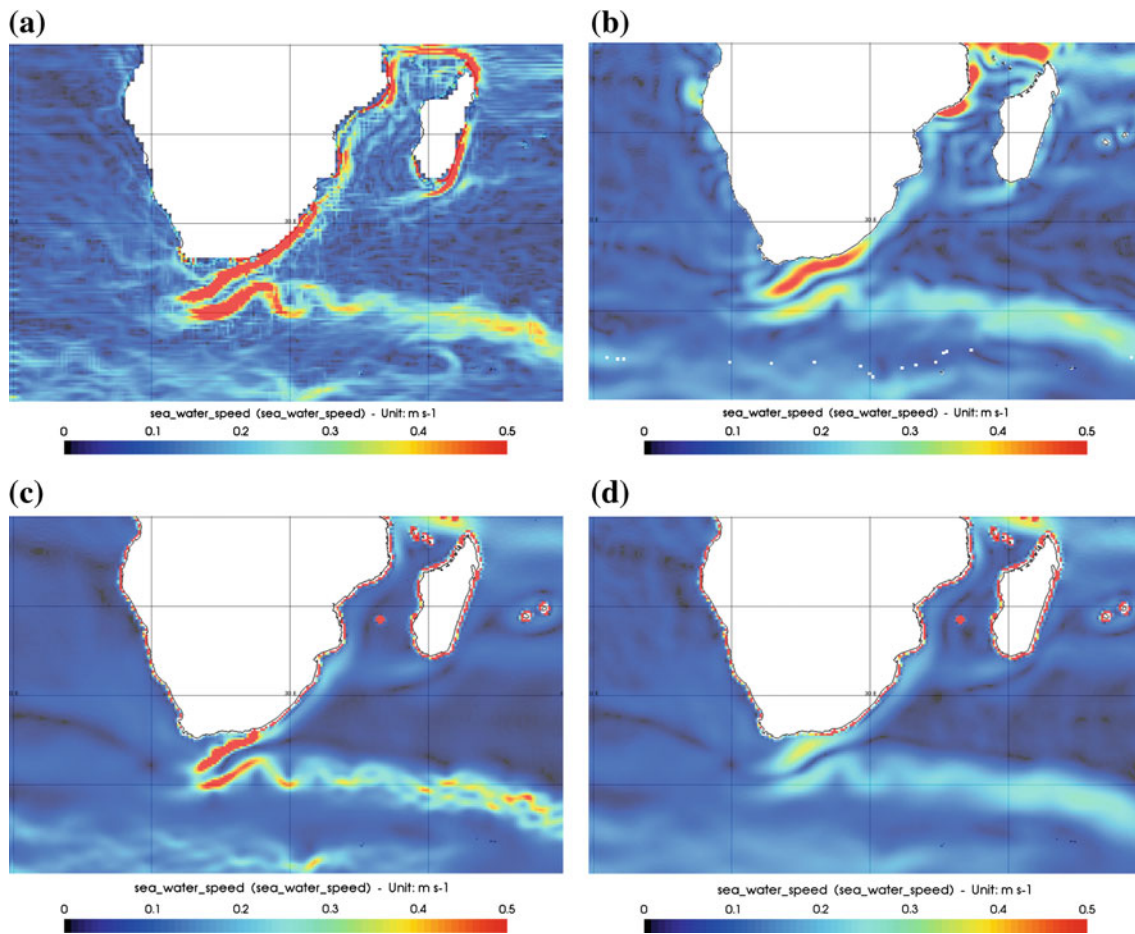


Fig. 18 The velocity speed of the ocean geostrophic surface currents computed from **a** the GUT a priori MDT_CNES_CLS_09, **b** the GUT a priori MDT_DTU10, and from the satellite-only MDT filtered using

c the nonlinear diffusion after 25 iterations, and **d** the linear diffusion after 20 iterations (detail in the Aghulas current area)

decision capability, which data and how much to preserve or to smooth.

In comparison with filtering of classical 2D or 3D images using the PDEs approach, filtering on closed surfaces has advantage that no boundary conditions are necessary. Numerical experiments show that both our filtering models conserve “mass”, i.e. an integral of the filtered data over whole computational domain, during all filtering steps. It confirms efficiency of the numerical schemes since the diffusion equations from their definitions should conserve a scalar quantity on the closed surface. This property makes the developed nonlinear Perona–Malik model suitable for data with an additive noise, where a mean value should be conserved. Another approach based on the mean curvature flow model is more appropriate for data where the noise has the so called “salt & pepper” character and should be reduced without requiring an overall conservation of mass. A development of such nonlinear filter is our plan for near future. We believe that the presented linear and nonlinear models of the diffusion filtering on closed surfaces will be helpful for better processing of various mea-

surements related to the Earth's surface and will contribute to correct interpretations of obtained results.

Acknowledgments The work has been supported by the Grant VEGA 1/1063/11, VEGA 1/0269/09 and the project APVV-0184-10.

References

- Alvarez L, Guichard F, Lions PL, Morel JM (1993) Axioms and fundamental equations of image processing. *Arch Ration Mech* 123(3):199–257
- Barrett R, Berry M, Chan TF, Demmel J, Donato J, Dongarra J, Eijkhout V, Pozo R, Romine C, Van der Vorst H (1994) Templates for the solution of linear systems: building blocks for iterative methods, 2nd edn. SIAM, Philadelphia. http://www.netlib.org/linalg/html_templates/Templates.html
- Bruinsma SL, Marty JC, Balmino G, Biancale R, Foerste C, Abrikosov O, Neumayer H (2010) GOCE gravity field recovery by means of the direct numerical method. Presented at the ESA living planet symposium, Bergen, Norway, 27th June–2nd July (2010). see also <http://earth.esa.int/GOCE>
- Capuzzo Dolcetta I, Ferretti R (2001) Optimal stopping time formulation of adaptive image filtering. *Appl Math Optim* 43(3):245–258

- Caselles V, Kimmel R, Sapiro G (1995) Geodesic active contours. In: Proceedings of the international conference on computer vision '95, Boston, pp 694–699
- Caselles V, Kimmel R, Sapiro G (1997) Geodesic active contours. *Int J Comput Vis* 22:61–79
- Catté F, Lions PL, Morel JM, Coll T (1992) Image selective smoothing and edge detection by nonlinear diffusion. *SIAM J Numer Anal* 29:182–193
- Chen Y, Vemuri BC, Wang L (2000) Image denoising and segmentation via nonlinear diffusion. *Comput Math Appl* 39:131–149
- Čunderlík R, Mikula K, Mojzeš M (2008) Numerical solution of the linearized fixed gravimetric boundary-value problem. *J Geod* 82: 15–29
- Dziuk G, Elliott CM (2007) Surface finite elements for parabolic equations. *J Comput Math* 25(4):385–407
- ESA (2011) The GOCE user toolbox, version 2.0. <http://earth.esa.int/gut>
- Kichenassamy S, Kumar A, Olver P, Tannenbaum A, Yezzi A (1995) Gradient flows and geometric active contours models. In: Proceedings of the international conference on computer vision '95, Boston
- Kichenassamy S, Kumar A, Olver P, Tannenbaum A, Yezzi A (1996) Conformal curvature flows: from phase transitions to active vision. *Arch Ration Mech Anal* 134:275–301
- Koenderink J (1984) The structure of images. *Biol Cybern* 50:363–370
- Mikula K (2002) Image processing with partial differential equations. In: Bourlioux A, Gander M (eds) *Modern methods in scientific computing and applications*. NATO science series II, vol 75. Kluwer, Dordrecht, pp 283–322
- Mikula K, Ramarosy N (2001) Semi-implicit finite volume scheme for solving nonlinear diffusion equations in image processing. *Numerische Mathematik* 89(3):561–590
- Pavlis NK, Holmes SA, Kenyon SC, Factor JK (2008) An earth gravitational model to degree 2160: EGM2008. Presented at the 2008 general assembly of EGU, Vienna, Austria, April 13–18
- Perona P, Malik J (1987) Scale space and edge detection using anisotropic diffusion. In: Proceedings of the IEEE society workshop on computer vision
- Witkin AP (1983) Scale-space filtering. In: Proceedings of the 8th international joint conference on artificial intelligence, Karlsruhe, Germany, vol 2, pp 1019–1022